

# Self-Sampling for Neural Point Cloud Consolidation

GAL METZER, Tel Aviv University

RANA HANOCKA, Tel Aviv University

RAJA GIRYES, Tel Aviv University

DANIEL COHEN-OR, Tel Aviv University

In this paper, we introduce a deep learning technique for consolidating and sharp feature generation of point clouds using only the input point cloud itself. Rather than explicitly define a prior that describes typical shape characteristics (*i.e.*, piecewise-smoothness), or a heuristic policy for generating *novel* sharp points, we opt to *learn* both using a neural network with shared-weights. Instead of relying on a large collection of manually annotated data, we use the self-supervision present within a single shape, *i.e.*, self-prior, to train the network, and learn the underlying distribution of sharp features specific to the given input point cloud. By learning to map a *low-curvature* subset of the input point cloud to a disjoint *high-curvature* subset, the network formalizes the shape-specific characteristics and infers how to generate sharp points. During test time, the network is repeatedly fed a random subset of points from the input and displaces them to generate an arbitrarily large set of novel sharp feature points. The local *shared* weights are optimized over the entire shape, learning non-local statistics and exploiting the recurrence of local-scale geometries. We demonstrate the ability to generate coherent sets of sharp feature points on a variety of shapes, while eliminating outliers and noise.

## 1 INTRODUCTION

Point clouds are a popular representation of 3D shapes. Their simplicity and direct relation to 3D scanners make them a practical candidate for a variety of applications in computer graphics. Point clouds acquired through scanning devices are a sparse and noisy sampling of the underlying 3D surface, which often have outliers or missing regions. Moreover, point sets impose innate technical challenges since they are unstructured, irregular, unordered and lack non-local information.

A fundamental challenge in the point cloud representation is the representation or generation of points with *sharp features*. Sharp features on 3D surfaces (*e.g.*, corners and edges) are sparse, yet they are a crucial cue in representing the underlying shape. Scanners struggle to accurately and thoroughly sample sharp regions. In particular, sharp regions on continuous surfaces contain high frequencies that cannot be faithfully reconstructed using finite and discrete samples. Thus, special attention is required to represent and reconstruct sharp features from imperfect data.

Several methods have been proposed to reconstruct point sets with sharp features. Classic approaches define a prior, such as piecewise smoothness, which characterize typical 3D shapes [Lipman et al. 2007; Huang et al. 2013; Xiong et al. 2014]. Recently, EC-NET [Yu et al. 2018a] present a deep learning technique for generating points with sharp features. Their approach is data-driven bypassing the need to define a prior, but rather it is learned through training examples. However, these examples are created by manually annotated sharp edges for supervision.

---

Authors' addresses: Gal Metzer, Tel Aviv University; Rana Hanocka, Tel Aviv University; Raja Giryes, Tel Aviv University; Daniel Cohen-Or, Tel Aviv University.

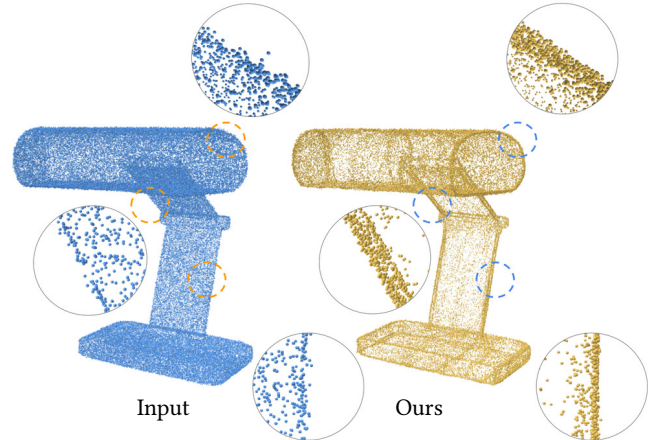


Fig. 1. Given a noisy input point cloud (blue), self-sample net consolidates and accurately sharpens its edges (gold).

In this work, we present a deep learning technique for generating points with sharp features using *only* a single given input point cloud. Instead of learning from a collection of manually annotated shapes, we leverage the inherent self-similarity present within a single shape. We train the network using self-supervision, by randomly selecting subsets of points from the input point cloud which are used to *implicitly* reconstruct the underlying surface. In particular, we sample a subset with *low-curvature* and learn a mapping to a disjoint subset of points with *high-curvature*. During inference, the generator is fed with a random subset of points from the input, which it displaces to synthesize novel sharp feature points. This process is repeated to obtain an arbitrarily large set of novel points with an emphasis on sharp feature points. Notably, since the prior is learned automatically from the input shape itself, there is no need to heuristically define strategies for generating *novel* sharp features.

Weight-sharing neural networks inherently encourage local-scale repetition in the generated points. Hanocka et al. [2020] coined the self-similarity learning *self-prior*, which we adopt here to indicate the innate prior learned from a single input shape. The shared-weights essentially encode the distribution of sharp feature points of a single shape, learning a self-prior for sharp feature generation. In particular, the network incorporates global statistics in the local kernel weights, since they are shared *globally* across the entire shape. The inductive bias of neural networks is remarkably effective at eliminating noise and outliers, a notoriously difficult problem in point cloud consolidation.

Learning internal statistics from a single image [Shocher et al. 2018; Shaham et al. 2019], or on single 3D shape [Williams et al.

2019; Hanocka et al. 2020; Liu et al. 2020], has demonstrated intriguing promise. In particular, self-prior learning offers considerable advantages compared to the alternate dataset-driven paradigm. For one, it does not require a supervised training dataset that sufficiently simulates the anticipated acquisition process and shape characteristics during *inference* time. Moreover, a network trained on a dataset can only allocate finite capacity to one particular shape. On the other hand, in the self-prior paradigm, the entire network capacity is solely devoted to *understanding* one particular shape. Given an input point cloud, the network implicitly learns the underlying surface and sharp feature regions, which are encoded in the network weights.

The premise of this work is that shapes are *not* random, they contain strong self-correlation across multiple scales, and can even contain recurring geometric structures (e.g., see Figure 1). The key is the internal network structure, which inherently models recurring and correlated structures, and therefore, ignores outliers and noise. In particular, our objective is to synthesize sharp feature points via a self-prior. However, the amount of sharp feature points in the input point cloud is scarce. We tackle this by re-balancing the point sample probability based on a local curvature approximation. This enables effectively learning the distribution of sharp feature points, despite their infrequent occurrence in the point set data.

We demonstrate results on a variety of shapes with varying amounts of sharp features. We show results on point sets with noise, non-uniform density and real scanned data without any normal information. In particular, we are able to accurately generate an arbitrarily large amount of points near sharp features, while eliminating outliers and noise.

## 2 RELATED WORK

In recent decades there is a wealth of works for re-sampling and consolidating point clouds. The early work of Alexa et al. [2001] uses a moving least square (MLS) operator to locally define a surface,

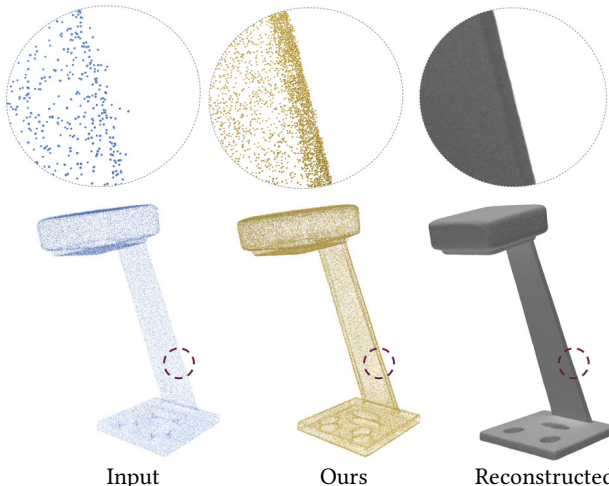


Fig. 2. Given a noisy input point cloud with outliers, self-sample net learns to consolidate and strengthen sharp features, which can be used to reconstruct a mesh surface with sharp features.

allowing up and down sampling points on the surface. Lipman et al. [2007] presented a locally optimal projection operator (LOP) to re-sample new points that are fairly distributed across the surface. Huang et al. [2009] have further improved this technique by adding an extra density weights term to the cost function, allowing dealing with non-uniform point distributions. These works have shown impressive results on scanned and noisy data, but they assume the surface is smooth and has no sharp features. To deal with piece-wise smooth surfaces that have sharp features, Haung et al. [2013] present a re-sampling technique that explicitly re-samples sharp features. Their technique builds upon the LOP operator and approximated normals iteratively introduces more points along the missing or sparsely sampled edge using the normals in the vicinity of the sharp feature.

Recently, with the emergence of neural networks new methods for point cloud re-sampling have been introduced. These methods build upon the ability of neural networks to learn from data. Processing point clouds is challenging since they are irregular and unordered, making it difficult to adopt the successful image-based CNN paradigm that assumes a regular grid structure [Qi et al. 2017a,b; Li et al. 2018; Wang et al. 2019]. A fundamental problem with these methods is that they are variant to rotations. To alleviate this problem rotation-invariant representations were proposed [Chen et al. 2019; Li et al. 2020]. In our work, we incorporate such rotation-invariant representation to facilitate self-similarity analysis.

Another related class of works deals with upsampling point clouds [Yu et al. 2018b; Yifan et al. 2019; Li et al. 2019]. These works operate on *patch-level*, which uses pairs of noisy / incomplete patches and their corresponding high-density surface sampled patches for supervision. To up-sample a point cloud, while respecting its sharp features, EC-Net [Yu et al. 2018a] learns from a dataset of meshes. The technique is trained to identify points that are on or close to edges and allows generating edge points during up-sampling. Their method, like the above up-sampling methods, are trained on large supervised datasets. Therefore, their performance is highly dependent on how well the training data accurately models the expected properties of the shapes during test time (*i.e.*, sub-sampling). Moreover, since these generators operate on local patches, they are unable to consider global self-similarity statistics during test time.

In contrast, our method is trained on the single input point cloud with self-supervision, and does not require modeling the specific acquisition / sampling process. Finally, the generator is *global*, since it generates a subset of the entire shape rather than patches, which encourages sharp features consistent with the characteristics of the entire shape.

The idea of using deep neural network as a prior has been studied in image processing [Ulyanov et al. 2018; Gandelsman et al. 2019]. These works show that applying CNNs directly on a low resolution or corrupt input image, can in fact learn to amend the imperfect input. Similar approaches have been developed for 3D surfaces [Williams et al. 2019; Hanocka et al. 2020], as a means to reconstruct a consolidated surface. Deep Geometric Prior (DGP) is applied on local charts and lacks global self-similarity abilities. Point2Mesh [Hanocka et al. 2020] builds upon MeshCNN [Hanocka et al. 2019] to reconstruct a watertight mesh containing global self-similarity through weight-sharing.

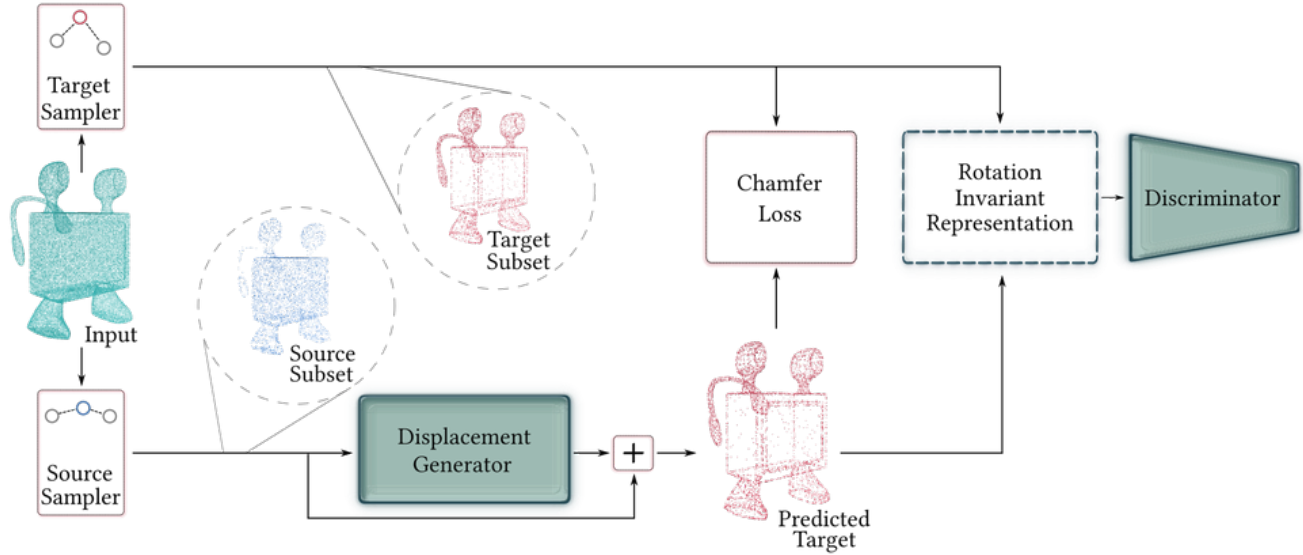


Fig. 3. Self-sample net training overview. We sample *source* and *target* subsets from the input point cloud, which contain mainly flat and sharp points, respectively. Then, the network learns displacement offsets which are added to the source subset, resulting in the predict target. The reconstruction loss uses a bidirectional Chamfer distance between the predicted target and target subset. The adversarial discriminator uses the target (*real*) and predicted target (*fake*) for training. In each training iteration, new source and target subsets are re-sampled from the input point cloud.

Our work shares similarities with a series of recent works that learn from a single input image [Ulyanov et al. 2018; Shocher et al. 2018; Zhou et al. 2018; Shaham et al. 2019]. These works downsample the input image or local patches and train a CNN to generate and restore the original image or patch, from the down-sampled version. Then the trained network is applied on the original data to produce a higher resolution or expanded output image containing the same features and patterns as the input. The rationale in these works is similar to ours. A generator is trained to predict the high feature details of a single input from sub-sampled versions, learning the internal statistics to map low detailed features to high detailed ones. In our work, we partition the input data, rather than down-sampling it, to balance out the sparse sharp features, and learn a mapping from low-curvature regions to high ones.

### 3 DEEP SHARP POINTS GENERATION

Self-sample net trains a network to generate a coherent set of points with sharp features using the self-supervision of the given input point cloud. The network is trained on samples of *source* and *target* subsets from the input point cloud, where we aim for the target subset to contain mainly *sharp* points. The generator receives the source subset as input, and displaces each point to predict a target subset. The generator is trained using a reconstruction loss (bidirectional Chamfer distance) between the target and predicted target subset, in addition to an adversarial loss.

Points in the input point cloud are defined as *sharp* based on a rough approximation of their local curvature, i.e., high curvature points. Since sharp points occur infrequently, we must re-balance the sampling probability of the target set to encourage selecting sharp

points more often. Since the generator regresses displacements that are relative to the source subset, the source and target subsets should be disjoint to avoid favoring the trivial solution (predicting zero offsets). Therefore, to ensure that the generator provides *meaningful* and non-zero offsets, the source subset sampler selects flat points (low curvature) with a high probability.

The discriminator is trained to distinguish between target subsets from the input point cloud (*real*) and the predicted target subsets (*fake*) estimated by the generator. This is used as an unsupervised loss to encourage the generator to create predicted sharp points that are indistinguishable from the distribution of sharp points in the input point cloud. To highlight local scale geometric repetitions across varying orientations, the discriminator operates on rotation invariant coordinates. Since these coordinates are agnostic to global orientation, they increase the redundancy within the sharp feature regions, which helps learn their underlying distribution.

Figure 3 illustrates the training procedure of self-sample net. After training is complete, the generator displaces subsets of the input point cloud to predict novel sharp feature points. This process is repeated to obtain an arbitrarily large set of novel sharp feature points (see Figure 7).

#### 3.1 Source and target point selection

We sample points from the input point cloud  $X$  to create source  $\mathbb{S}$  and target  $\mathbb{T}$  subsets. We aim for the target to contain mostly sharp feature points from the input point cloud. On the other hand, the source subset should contain mostly flat points. However, since point sharpness is unknown *a priori*, we define a proxy for sharpness via a rough approximation of local curvature. The estimated curvature

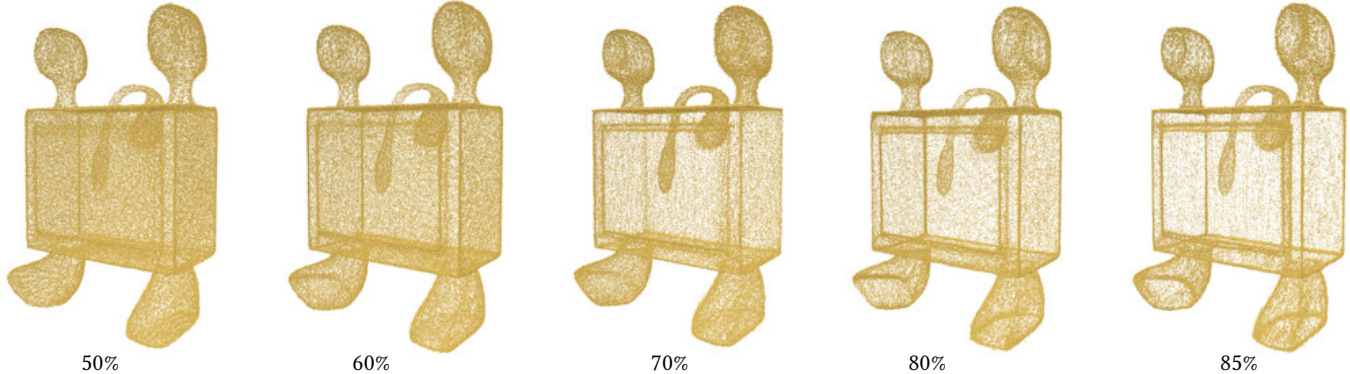


Fig. 4. Results of training on different percentages of *curvy* points ( $p_T$ ) in the sampled target subsets. Increasing the amount of curvy points in the target subsets results in a sharper predicted output (e.g., 85%), whereas less curvy points (e.g., 50%) results in a more uniform output.

is used to define different sampling probabilities for both the source and target sets. Note, that while it is possible to define alternative methods for sharpness approximation, we observe in practice that a simple policy for estimating curvature using only point positions (*i.e.*, assuming normals are not given) produces favorable results.

Approximating the curvature of each point starts by estimating the point normals using a simple plane fitting technique. We calculate the difference in normal angles for each point and its  $k$ -nearest neighbors ( $kNN$ ). The estimated curvature of a point is given by summing all angle differences with each of its  $k$  neighbors. Finally, using a simple threshold on these curvatures, the points are classified as either *curvy* or *flat*. In practice, we estimate the *curvy threshold*  $\tau$  by the mean angle difference. Figure 5 demonstrates the  $kNN$  curvature on a few input point clouds.

Each point and its associated *curvy* class are used to sample and create the training source and target subsets  $S, T \in \mathbb{R}^{m \times 3}$  from the input point cloud  $X \in \mathbb{R}^{n \times 3}$  (where  $m < n$ ). The probability of sampling a curvy point in the source and target subset is given by a binary (Bernoulli) distribution with probabilities  $p_S$  and  $p_T$ , respectively. Naturally, we set the probability for drawing a curvy point in the target to be high, while the probability for a curvy point in the source is low,  $0 \leq p_S \leq p_T \leq 1$ . Finally, we sample each point in the curvy or flat class with uniform probability. Each time we create a new source and target subset pair, we ensure that they are disjoint  $S \cap T = \emptyset$ . The effect of training using varying  $p_T$  is shown in Figure 4.

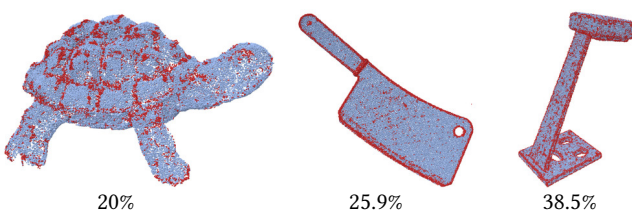


Fig. 5. Visualization of the points classified as *curvy* for different point clouds. The  $kNN$  curvature was thresholded by the mean curvature, which results in a percentage of shape points which is *sensitive* to the amount of sharp features in the input point cloud.

### 3.2 Network structure

The generator and discriminator are both comprised of a fully-convolutional point network. In this work, we use PointNet++ [Qi et al. 2017b], which provides the fundamental neural network operators for irregular point cloud data.

The generator  $G$  receives a source subset  $S \in \mathbb{R}^{m \times 3}$  and outputs a displacement vector in  $\Delta \in \mathbb{R}^{m \times 3}$  which is added to  $S$ , resulting in the predicted target  $\hat{T} = S + \Delta$ . The generator is trained using a *reconstruction* loss, which compares the predicted target  $\hat{T}$  to a target subset  $T \in \mathbb{R}^{m \times 3}$ . The adversarial loss is used to alternatively train the generator and discriminator.

Each point in the source has a 3-dimensional  $< x, y, z >$  coordinate associated with it, which is lifted by the generator to a higher dimensional feature space through a series of convolutions, non-linear activation units and normalization layers. Each deep feature per point is eventually mapped to the final 3-dimensional vector, which displaces the corresponding input source point to a point which lies on the manifold of target (sharp) shape features. We initialize the last convolutional layer to output near-zero displacement vectors, which provides a better initial condition and therefore more efficient learning.

### 3.3 Reconstruction Loss

The reconstruction loss is given by the bi-directional Chamfer distance between the target  $T$  and predicted target  $\hat{T}$  subsets, which is differential and robust to outliers [Fan et al. 2017]. The chamfer distance between two point sets  $P$  and  $Q$  is given by:

$$d(P, Q) = \sum_{p \in P} \min_{q \in Q} \|p - q\|_2^2 + \sum_{q \in Q} \min_{p \in P} \|p - q\|_2^2. \quad (1)$$

The Chamfer distance is invariant to point *ordering*, which avoids the need to define correspondence. Instead, the network *independently* learns to map source points to the underlying target shape distribution. Since there is no correspondence, it is important that each pair of source and target subsets  $S, T$  are disjoint, which helps avoid the trivial solution of no-displacement (*i.e.*,  $\Delta = \vec{0}$ ).

### 3.4 Adversarial loss

In addition to the reconstruction loss, we incorporate an adversarial loss, by training a discriminator. Prior to the discriminator, each point in the target and predicted target  $\mathbb{T}, \hat{\mathbb{T}} \in \mathbb{R}^{m \times 3}$  is transformed into a rotation invariant feature using [Chen et al. 2019]. This feature-transform  $\mathcal{F}$  helps the discriminator to capture local scale geometric details by highlighting redundancies across multiple orientations. The rotation invariant features are built from the  $k$ NN for each point and the center of mass of the entire point cloud, which results in a  $3 \cdot k + 1$  dimensional rotation invariant feature vector per point. In other words, we have  $\mathcal{F}(\mathbb{T}), \mathcal{F}(\hat{\mathbb{T}}) \in \mathbb{R}^{m \times 3 \cdot k + 1}$ .

The discriminator  $D$  is trained using the WGAN-GP loss [Gulrajani et al. 2017]. Similar to the generator architecture, the discriminator maps each (rotation-invariant) point to a higher-dimensional

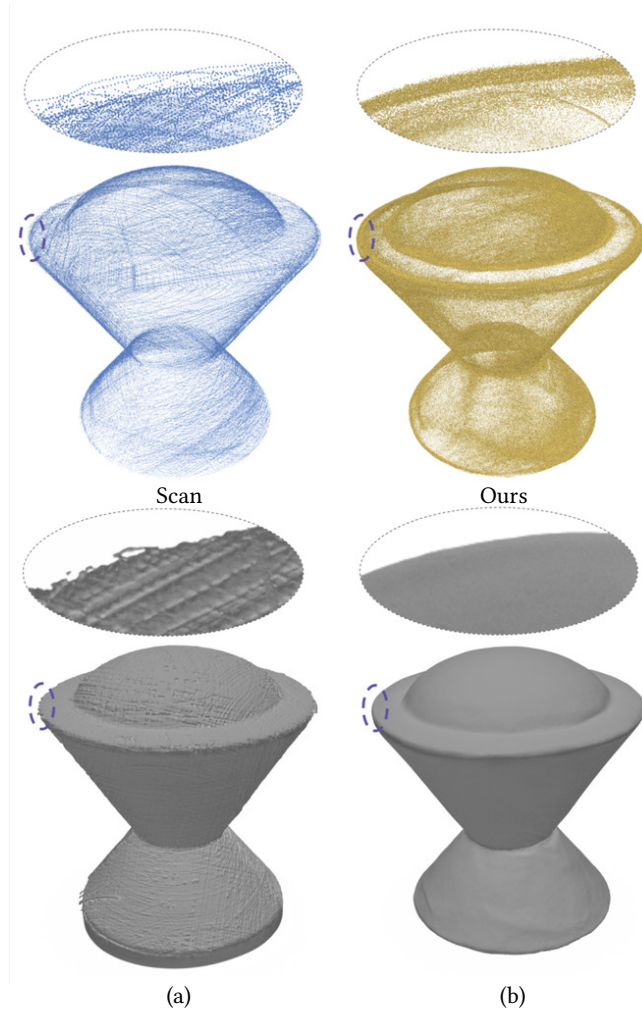


Fig. 6. Scanned input contains artifacts which self-sample net removes while preserving sharp features. Reconstructing a surface directly from the scanned input (a) yields an undesirable reconstruction, whereas reconstructing the surface directly from the output of self-sample net (b) leads to favorable results.

feature space via a series of convolutions, non-linear activations and normalization layers. The adversarial deep point features are mapped to an output with dimensions  $m \times 1$ . The generator and discriminator are trained in an alternate manner using the same loss functions as in [Gulrajani et al. 2017]. During the discriminator iteration, the loss is given by

$$L_D(\mathbb{T}, \hat{\mathbb{T}}) = \frac{1}{m} \sum_{\hat{t} \in \hat{\mathbb{T}}} D(\mathcal{F}(\hat{t})) - \frac{1}{m} \sum_{t \in \mathbb{T}} D(\mathcal{F}(t)), \quad (2)$$

which maximizes the per-point feature activation in the target subset and minimizes per-point feature activation in the predicted target subset. During the generator iteration, the same loss is maximized, i.e., the generator minimizes

$$L_{adv}(\hat{\mathbb{T}}) = -\frac{1}{m} \sum_{\hat{t} \in \hat{\mathbb{T}}} D(\mathcal{F}(\hat{t})). \quad (3)$$

Adding it to the Chamfer distance discussed above, the generator loss is given by

$$L_G = d(T, \hat{\mathbb{T}}) + \alpha \cdot L_{adv}(\hat{\mathbb{T}}) \quad (4)$$

In addition, we use the gradient penalty (GP), which was shown in [Gulrajani et al. 2017] to improve the training of WGANs. The GP enforces the Lipschitz constraint via the gradient of the discriminator when applied to some interpolation between real and fake samples (*i.e.*,  $(1 - \lambda) \cdot \mathbb{T} + \lambda \cdot \hat{\mathbb{T}}$ ). While this interpolation is trivial in images, for unordered point clouds there is no correspondence between  $\mathbb{T}$  and  $\hat{\mathbb{T}}$ . To this end, we use

$$L_{GP}(z) = (\|\nabla_z D(z)\|_2 - 1)^2, \quad (5)$$

where  $z$  alternates between  $z = \mathbb{T}$  and  $z = \hat{\mathbb{T}}$ . This enables encouraging both gradients to have an  $\ell_2$ -norm of one, without the need for correspondence.

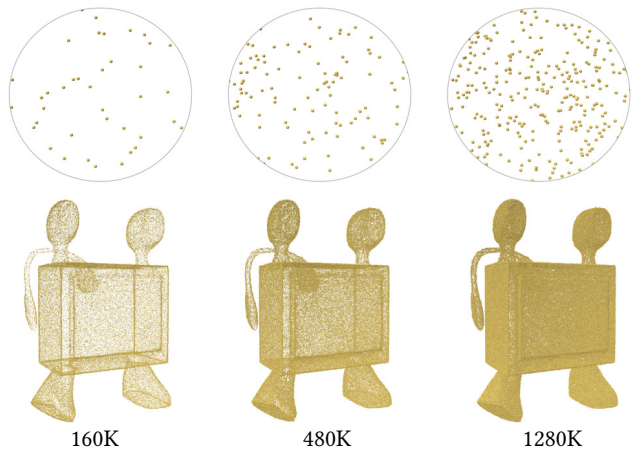


Fig. 7. Generating a consolidated point cloud at arbitrary resolutions. Observe how increasing the number of points creates greater coverage on the shape surface, rather than simply generating the same points on top of each other.

### 3.5 Inference

After training is complete, the generator has successfully learned the underlying distribution of the target point features. During inference, the generator displaces subsets from the input point cloud to create novel points which are part of the distribution of the target (sharp) features. This process is repeated to achieve an infinitely large amount of samples on the underlying surface. Due to the large network capacity and rich feature representation, novel points can be generated as a function of their input subset. For a given point in the input point cloud  $x \in X$ , we can generate a *large* variety of target feature points based on the variety of points in the input subset. Therefore, by combining the results of  $k$  different subsets of size  $m$ , we obtain an up-sampled version of the input of size  $k \cdot m$ .

*Output Sampling Density.* A key feature of self-sample net is that the consolidated point cloud can be generated at an arbitrarily large resolution. More specifically, we randomly sample a set of input points from the point cloud,  $\langle x_i, x_j, x_k, \dots \rangle \in X$ , which generate offsets  $\langle \Delta_i, \Delta_j, \Delta_k, \dots \rangle$  that are added back to the input points resulting in the novel samples  $\langle x_i + \Delta_i, x_j + \Delta_j, x_k + \Delta_k, \dots \rangle$ . For a particular point  $x_i$ , the corresponding offset  $\Delta_i$  generated by the network  $G$  is a function of the input samples, i.e.,  $\Delta_i = G(\langle x_i, x_j, x_k, \dots \rangle)$ . In other words, we can generate a variety of different outputs, based on sampling different input subsets since  $\Delta_i = G(\langle x_i, x_j, x_k, \dots \rangle) \neq G(\langle x_i, x_l, x_m, \dots \rangle)$ . Figure 11 demonstrates the diversity of such an output set of points (yellow) for a given input point (red) with different subsets as input. Notably, increasing the number of output points generates greater coverage on the underlying surface, without generating redundant points. To see this further, observe how increasing the resolution in Figure 7 results in a denser sampling. Indeed, this is possible since each time a different subset is sampled from the input point cloud, a different set of output points is generated.

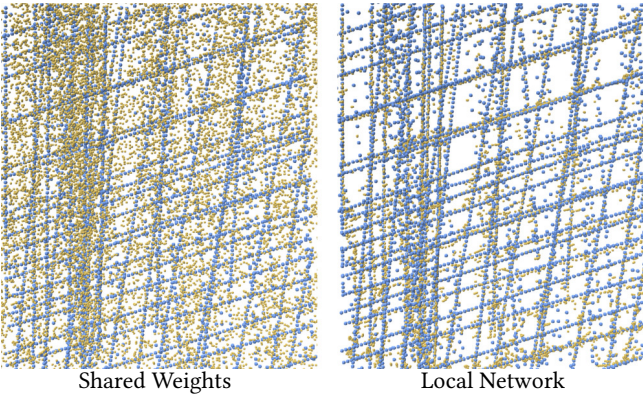


Fig. 8. Training a local network on a patch of the input (right) compared with training the network from subsets across the input point cloud. Observe how when training on a single patch the network overfits to the data. On the other hand, when trained on the entire shape it generalizes well by sampling the underlying surface.

## 4 EXPERIMENTS

To validate the ability of self-sample net, we conduct a series of qualitative and quantitative experiments. We demonstrate results on a variety of different shapes, which may contain noise, outliers and non-uniform point density on synthetic and real scanned data. We compare to EC-Net [Yu et al. 2018a], which is an edge aware deep neural method for point cloud consolidation, and EAR [Huang et al. 2013]. Unless otherwise stated, all results in this paper are the direct output from the network, without any pre-processing to the input point cloud or the output point cloud.

### 4.1 Weight Sharing

We claim that neural networks with weight-sharing abilities posses an inductive bias which enables self-sample net to ignore noise and outliers and complete low density regions. This is in contrast to multiple *local* networks which operate on small patches, without any global context or shared information among different patches. To validate this claim, we train a single global network (which shares the same weights for all inputs) and multiple local networks on a synthetic cube which has missing samples near some corners and edges. The single global network is trained on the entire cube. We separate the cube into 8 octants, and train 8 different local networks on each octant. In order to provide each local network with as much data as the single global network, we provide 8 $\times$  as many points to each octant. Figure 9 shows the results. Despite using 8 $\times$  as many points (in total) and 8 $\times$  as many networks, the local networks easily overfit the missing regions. In particular, notice the cube corner. On the other hand, the shared weights exploit the redundancy present in a single shape, and encourages a plausible solution.

We perform another comparison on a real scan from AIM@SHAPEVISIONAIR. In this setup, we train a single local network on an extracted patch from the scan. The result is shown in Figure 8. As expected, the local network overfits the artificial pattern from the input scan. For reference, we included the result from the global network that was trained on the entire shape.

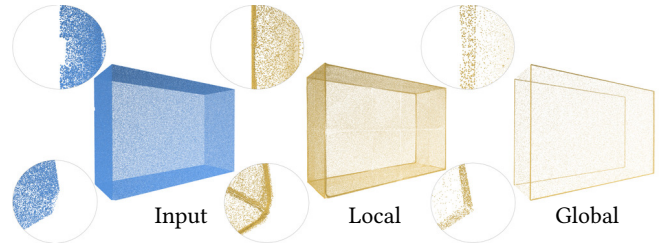


Fig. 9. The power of global shared weights. When using a single global trained on the entire shape, the network weights learn to share information across multiple scales. The shared global statistics are a powerful prior for completing a sharp corner. On the other hand, we divide the cube into 8 separate parts, and train 8 different *local* networks to upsample the inputs from each octant. Note that we increased the number of points in each octant to give the local network a significant advantage (8 $\times$  as many points). The local scheme was provided more data and 8 $\times$  as many networks, but since the weights are unshared, they lack crucial global information.

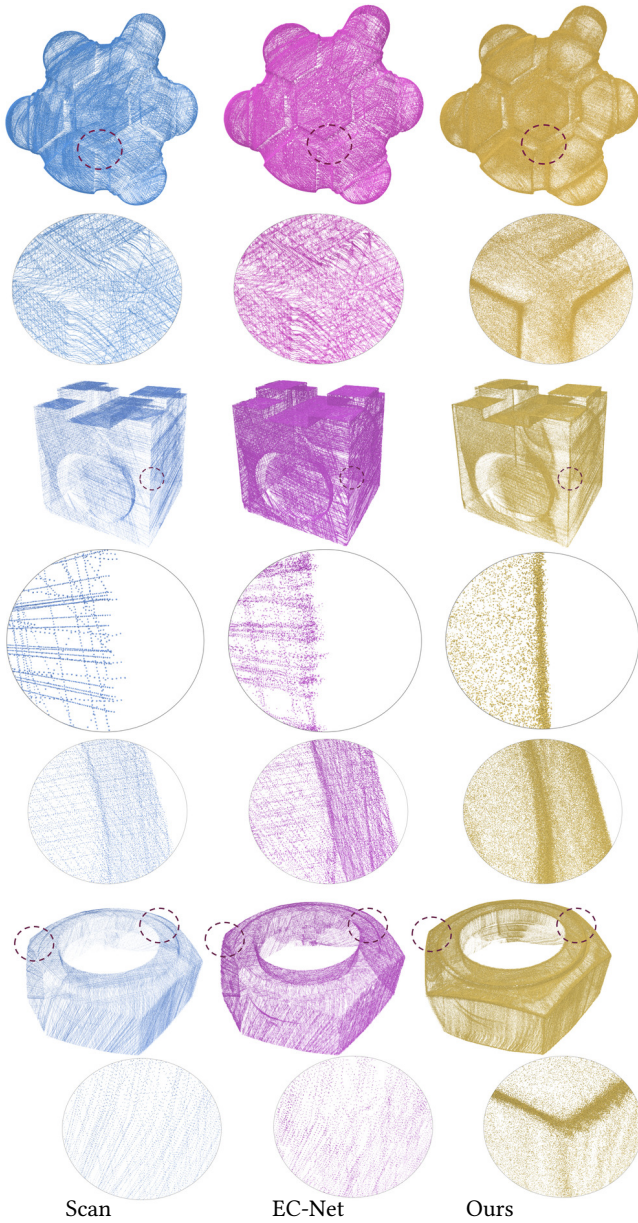


Fig. 10. Real 3D scans from AIM@SHAPE-VISIONAIR. Observe how self-sample net is agnostic to the unnatural pattern in the input point cloud, by producing a dense consolidated point set with sharp features.

#### 4.2 Output Point Set Distribution

Figure 11 helps illustrate what the network has learned and the type of diverse output samples it can produce. We selected five (constant) points (red) from the input point cloud (blue), and concatenated them into many random subsets selected during the up-sampling process. Each of the output points (colored in yellow) were produced by different subsets of the input point cloud.

Observe that the network learns the underlying distribution of the surface during training time, such that during inference an

input point can be mapped to many novel output points, which densely sample the underlying surface. Note the top left inset, which highlights the network’s ability to capture the distribution of an edge, despite the unnatural sampling in the scanned data. Moreover, in the bottom inset, new points are densely generated along the edge boundary of the object, yet, do not surpass the edge itself (remain contained on the surface).

The amount of points generated on sharp features can be controlled via the sampling probability of curvy points in the target subset  $p_T$ . As shown in Figure 16, this directly affects the displacement magnitude of each input point. For example, when  $p_T$  is high (e.g.,  $p_T = 85\%$ ), the network generates large displacements for points on flat surfaces.

#### 4.3 Real Scans

We ran self-sample net on real scans provided by AIM@SHAPE-VISIONAIR. Figure 6 demonstrates the ability of self-sample net to generate sharp and accurate edges corresponding to the underlying shape, despite the presence of unnatural scanner noise. In addition, applying surface reconstruction directly to the input point cloud leads to undesirable results with scanning artifacts and non-sharp edges. On the other hand, reconstructing a surface from the consolidated output of the network leads to pleasing results, with sharp edges. Note that we did not apply any post-processing to our point cloud, however, we did use an off-the-shelf tool in MeshLab to estimate the point cloud normals.

Figure 10 shows additional results on real scans from AIM@SHAPE-VISIONAIR with a comparison to EC-Net. Observe how self-sample

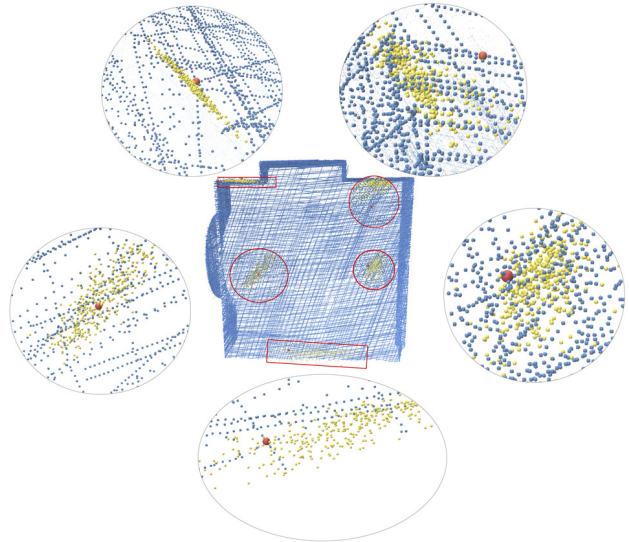


Fig. 11. Diversity in novel sharp feature generation. Given an input point (red) and random subsets from the input point cloud (entire point cloud in blue), our network generates different displacements which are added to the input point to generate a variety of different output points (yellow). In other words, novel points on the surface are *conditioned* on selected input subset.

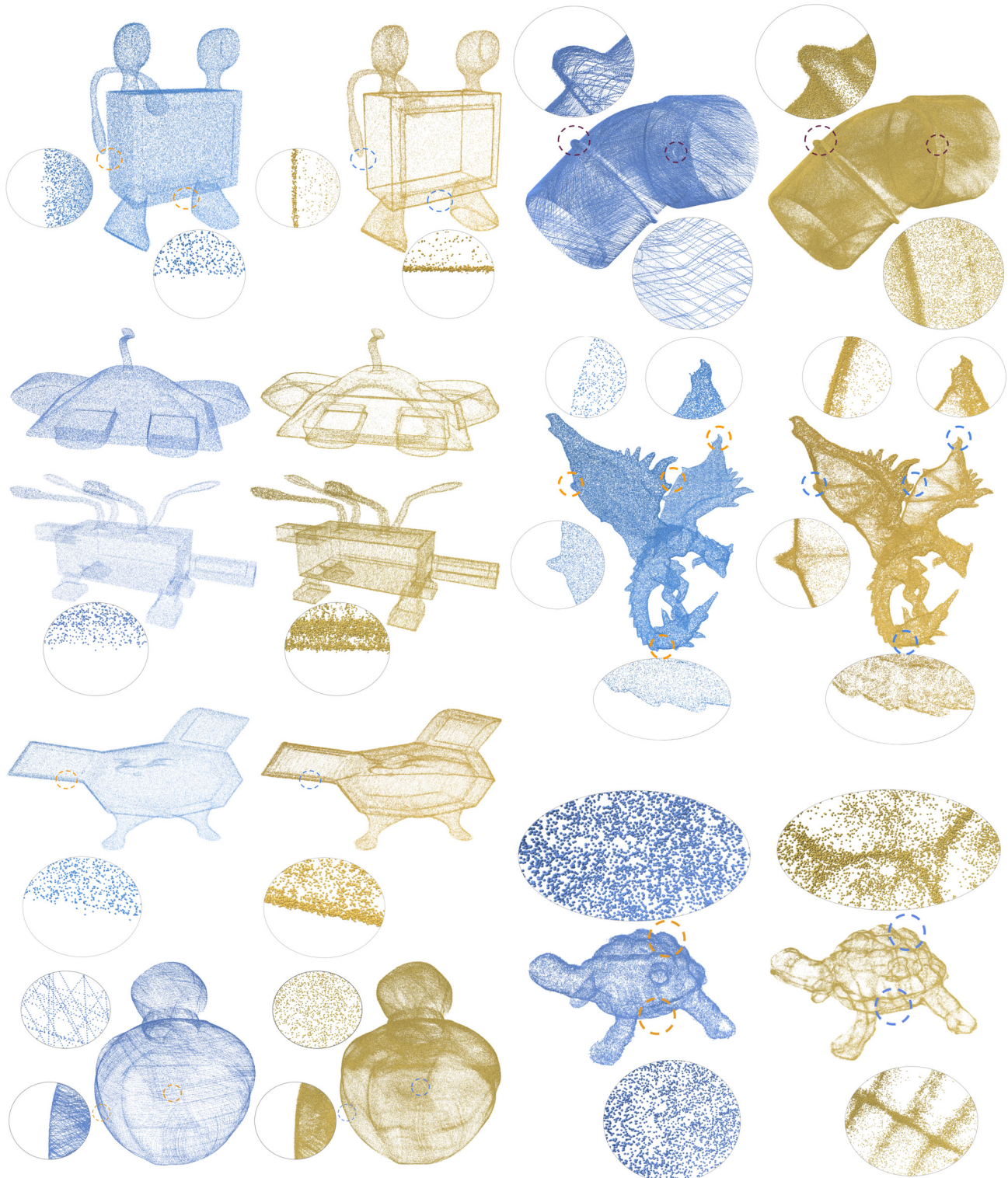


Fig. 12. Additional results on real and synthetic scans.

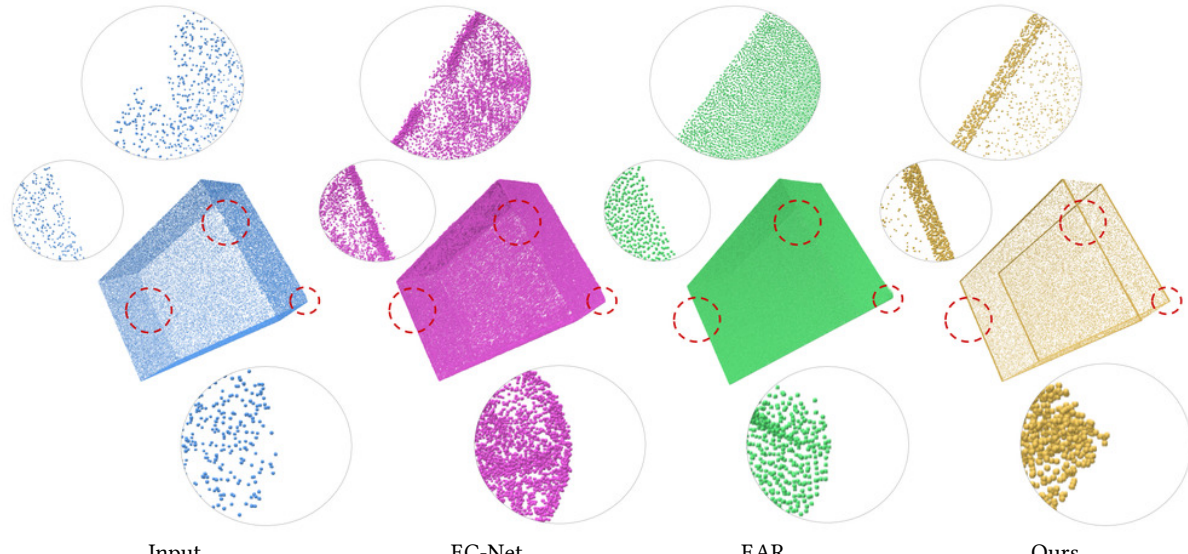


Fig. 13. Input point cloud with missing samples on sharp features. The results shown are the outputs from EC-Net (without edge selection), EAR and our network. Our results are the direct result of the network, without any pre/post processing.

net is able to learn the underlying surface of the object despite the artificial scanning pattern. Moreover, it produces a dense consolidated point set with sharp features. On the other hand, since EC-Net was not trained on such data, it is sensitive to this particular sampling and generally preserves the artificial scanning pattern in the output. Additional results of self-sample net on real scans can be found in Figure 12.

#### 4.4 Comparisons

We performed additional qualitative comparisons to EAR and EC-Net. Figures 13 and 14 highlights where self-sample net reconstructs sharp points in a better way compared to these approaches. In particular, the weight-sharing property enables consolidating sharp regions and ignoring noise and outliers. For example, in Figure 13 self-sample net completes the corner with many sharp points, where the alternative approaches have rounder corners.

We perform a quantitative comparisons on the benchmark of EC-Net [Yu et al. 2018a], which includes eight virtually scanned

objects. We use the F-score metric [Knapitsch et al. 2017; Hanocka et al. 2020], which is the harmonic mean between the precision and recall at some threshold  $\tau$ :

$$F(\tau) = \frac{2P(\tau)R(\tau)}{P(\tau) + R(\tau)}. \quad (6)$$

The F-score is computed with respect to an edge-sampled version of the ground-truth mesh, to indicate how accurately the estimated point samples lie on edges ( $P(\tau)$ ), as well as how well all edges have been covered ( $R(\tau)$ ).

We use an edge-aware sampling method for the ground-truth meshes to emphasize sharp edges in the quantitative comparisons. An edge on the mesh is considered sharp if its dihedral angle is small. We select edges based on their sharpness and length. After an edge is selected, we sample points on the edge adjacent faces with high probability, and with a decreasing probability when moving away from the edge (*i.e.*, using a sort of triangular Gaussian distribution).

Table 1 presents the F-score metrics for self-sample net, and two variations of EC-Net provided in the authors reference implementation (edge selected and all output points). On the left side of Table 1 we show an example from the benchmark: input point cloud (blue), self-sample net (yellow) and EC-Net (all points) in purple. Another example from the benchmark is presented in Figure 17. It should be noted that our method does not use any pre or post processing on the input or output point cloud. The above qualitative and quantitative comparisons indicate that self-sample net achieves on-par or better results compared to EC-Net despite being trained only on the input shape.

Shape	ours	EC-E	EC-A
camera	<b>98.49</b>	87.59	94.52
fandisk	<b>99.86</b>	85.97	99.02
switch pot	<b>99.26</b>	90.51	89.62
chair	<b>99.99</b>	97.15	<b>99.99</b>
table	<b>99.59</b>	97.11	95.42
sofa	68.67	<b>85.95</b>	77.92
headphone	<b>99.96</b>	98.91	<b>99.96</b>
monitor	<b>99.92</b>	71.17	99.7

Table 1. F-score comparison on the EC-Net dataset. The F-score is w.r.t. to the ground-truth *edge sampled* mesh. Results reported for self-sample net, EC-Net edge points (EC-E), and EC-Net all points (EC-A).

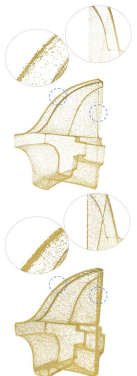


Fig. 14. Comparison to EAR [2013] on Figure 1

Shape	PointNet++		PointNet	
	RotInv	XYZ	RotInv	XYZ
fandisk	<b>98.25</b>	86.85	97.72	94.57
headphone	99.03	97.79	<b>99.15</b>	96.45
sofa	<b>88.14</b>	71.03	80.4	30.48
camera	75.78	65.08	80.44	<b>82.1</b>
switch pot	<b>95.08</b>	81.95	94.17	65.4
table	80.56	<b>83.96</b>	81.54	80.59
chair	<b>98.34</b>	95.71	98.33	92.73
monitor	<b>93.3</b>	81.6	90.0	70.24

Table 2. Ablation study. Left: results obtained from PointNet (top) and PointNet++ (bottom). Note how PointNet++ captures more sharp edges.

#### 4.5 Ablation Study

We perform an ablation study, to help analyze the role of different components in our framework. We adopt the same setup as previously, but use uniformly sampled point clouds from the shapes in [Yu et al. 2018a] (instead of virtually scanned), to help demonstrate the ability of self-sample net on different sampling patterns. We compare PointNet to PointNet++, with and without the use of the rotation invariant features in the discriminator, on all the shapes in Table 1. As expected, the rotation invariant features in the discriminator with PointNet++ are generally better than using Cartesian coordinates in the discriminator with PointNet. We believe this stems from the fact that PointNet++ better represents point clouds with its hierarchical architecture, compared to the single global max pool in PointNet.

#### 4.6 Implementation Details

Our implementation uses the following software: Polyscope [Sharp et al. 2019], PyTorch [Paszke et al. 2017], FAISS [Johnson et al. 2017] and PointNet++ PyTorch [Wijmans 2018]. Runtimes for our implementation are: 5, 6, and 3.8 hours for a single model for the AIM@SHAPE-VISIONAIR scans, Table 1 and alien shapes, respectively. If we only use the Chamfer loss, runtimes correspond to: 60,

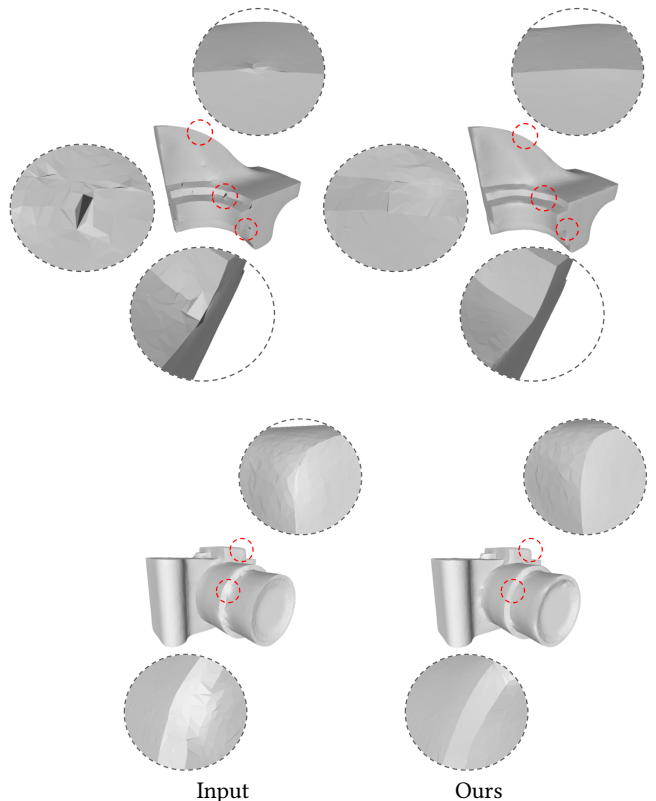


Fig. 15. Reconstruction from the input point cloud (left), and reconstruction on the output of our method. Observe how consolidation removes noise and preserves sharp features. Mesh reconstruction was performed using [Bernardini et al. 1999], and [Sun et al. 2007].

16, and 50 minutes, respectively. Point clouds with larger resolutions require longer runtimes.

We use the default hyper-parameters provided by the PointNet++ Pytorch implementation [Wijmans 2018] for the segmentation task. We selected the subset size in each iteration to be around 5 – 10% of the input point cloud. In general, the network is insensitive to the particular subset size. An input point cloud is considered sparse if it has less than 20k points (much smaller than the amount of points typically obtained in a real scan). In this case, there may not be enough sharp points present in 5 – 10% of the data. To this end, 5 – 10% subsets on low resolution point clouds should be sampled uniformly instead of with curvature (see such results in the supplemental material).

## 5 CONCLUSIONS

We have presented a novel concept of curvature-based sampling for sharp point cloud generation. Self-sample net proposes training a neural network only on the input point cloud, achieving remarkable performance, which outperforms both classic techniques and large dataset-driven learning. We believe that this strategy has the potential to extend beyond the generation of sharp features, by employing other task-driven sampling patterns.

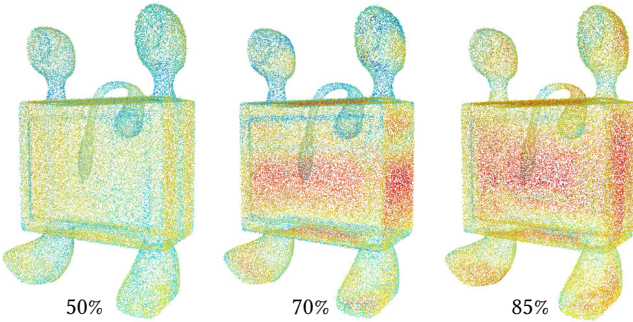


Fig. 16. Heatmap visualization of the network predicted displacements on an input point cloud. We train self-sample net using different percentages of *curvy* points in the sampled target subsets (results in Figure 4). Red and blue are for large and small displacements, respectively. Re-weighting the target sampling probability  $p_T$ , in order to include more curvy points implicitly encourages the network to predict larger displacements. Observe how the network trained with  $p_T = 85\%$  displaces the input points inside large flat regions the furthest away.

The network used in this work is trained on the input data itself and infers novel points that densify and enhance the global geometric coherency of sharp features. self-sample net leverages the inductive bias of neural networks which leads to a globally consistent solution. The network's ability stems from the global weight-sharing, which helps prevent *overfitting*. As we have shown, the weight-sharing learns common local geometries across the whole shape, which allows amending erroneous regions, beyond denoising.

A limitation of this approach is the run-time during inference. This technique is significantly slower than a pre-trained network or classic techniques. As learning on irregular structures becomes more mainstream and optimized (e.g., recently released packages Kaolin [Murthy et al. 2019] and PyTorch3D [Ravi et al. 2020]), run-time will improve significantly.

The focus of this work is generating sharp feature points. It should be emphasized that these features are typically sparse, which can be problematic for neural networks since they tend to ignore sparse data and focus on learning the core data modes. In this work, we compensated for the sparsity of sharp points by using a biased subsampler that re-balances the probability of sparse regions in the

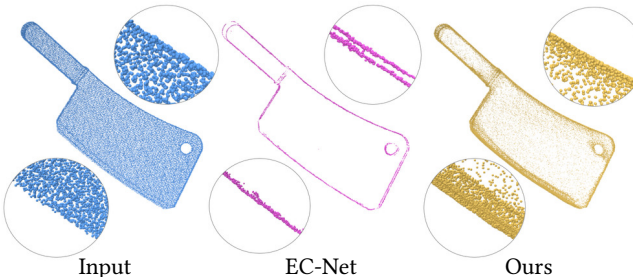


Fig. 17. Using simulated scanned point cloud as input (from [Yu et al. 2018a]), results of self-sample net and the edge selected output from EC-Net. Results are directly output from the networks (without any pre/post processing).

target subset, which facilitates learning sharp features. Note that our method does not require parameter tuning, and is generally robust to hyper-parameters.

In the future, we would like to consider extending the method to learn local geometric motifs, for example, on decorative furniture or other artistic fixtures. Learning geometric motifs can be challenging since they typically have low prevalence in a single shape, and are often unique across various shapes. Another interesting avenue is learning to transfer sharp features between shapes, possibly between different modalities, e.g., from 3D meshes to scanned point clouds or vice versa. We are also considering using the self-prior for increasing self-similarities within a single shape, as means to enhance the aesthetics of geometric objects.

## REFERENCES

- Marc Alexa, Johannes Behr, Daniel Cohen-Or, Shachar Fleishman, David Levin, and Claudio T Silva. 2001. Point set surfaces. In *Proceedings Visualization, 2001. VIS'01*. IEEE, 21–29.
- Fausto Bernardini, Joshua Mittleman, Holly Rushmeier, Cláudio Silva, and Gabriel Taubin. 1999. The ball-pivoting algorithm for surface reconstruction. *IEEE transactions on visualization and computer graphics* 5, 4 (1999), 349–359.
- Chao Chen, Guanbin Li, Ruijia Xu, Tianshui Chen, Meng Wang, and Liang Lin. 2019. ClusterNet: Deep hierarchical cluster network with rigorously rotation-invariant representation for point cloud analysis. In *Proceedings of the IEEE Conference on Computer Vision and Pattern Recognition*. 4994–5002.
- Haoqiang Fan, Hao Su, and Leonidas J Guibas. 2017. A point set generation network for 3d object reconstruction from a single image. In *Proceedings of the IEEE conference on computer vision and pattern recognition*. 605–613.
- Yossi Gandalzman, Assaf Shoher, and Michal Irani. 2019. "Double-DIP": Unsupervised Image Decomposition via Coupled Deep-Image-Priors. (6 2019).
- Ishaan Gulrajani, Faruk Ahmed, Martin Arjovsky, Vincent Dumoulin, and Aaron C Courville. 2017. Improved training of wasserstein gans. In *Advances in neural information processing systems*. 5767–5777.
- Rana Hanocka, Amir Hertz, Noa Fish, Raja Giryes, Shachar Fleishman, and Daniel Cohen-Or. 2019. MeshCNN: A Network with an Edge. *ACM Trans. Graph.* 38, 4, Article 90 (July 2019), 12 pages. <https://doi.org/10.1145/3306346.3322959>
- Rana Hanocka, Gal Metzer, Raja Giryes, and Daniel Cohen-Or. 2020. Point2Mesh: A Self-Prior for Deformable Meshes. *ACM Trans. Graph.* 39, 4 (2020). <https://doi.org/10.1145/3386569.3392415>
- Hui Huang, Dan Li, Hao Zhang, Uri Ascher, and Daniel Cohen-Or. 2009. Consolidation of unorganized point clouds for surface reconstruction. *ACM transactions on graphics (TOG)* 28, 5 (2009), 176.
- Hui Huang, Shihao Wu, Minglun Gong, Daniel Cohen-Or, Uri Ascher, and Hao Richard Zhang. 2013. Edge-aware point set resampling. *ACM transactions on graphics (TOG)* 32, 1 (2013), 9.
- Jeff Johnson, Matthijs Douze, and Hervé Jégou. 2017. Billion-scale similarity search with GPUs. *arXiv preprint arXiv:1702.08734* (2017).
- Arno Knapitsch, Jaesik Park, Qian-Yi Zhou, and Vladlen Koltun. 2017. Tanks and Temples: Benchmarking Large-Scale Scene Reconstruction. *ACM Transactions on Graphics* 36, 4 (2017).
- Ruihui Li, Xianzhi Li, Chi-Wing Fu, Daniel Cohen-Or, and Pheng-Ann Heng. 2019. PU-GAN: A Point Cloud Upsampling Adversarial Network. In *IEEE International Conference on Computer Vision (ICCV)*.
- Xianzhi Li, Ruihui Li, Guangyong Chen, Chi-Wing Fu, Daniel Cohen-Or, and Pheng-Ann Heng. 2020. A Rotation-Invariant Framework for Deep Point Cloud Analysis. *arXiv preprint arXiv:2003.07238* (2020).
- Yangyan Li, Rui Bu, Mingchao Sun, Wei Wu, Xinhuan Di, and Baoquan Chen. 2018. Pointcnn: Convolution on x-transformed points. In *Advances in neural information processing systems*. 820–830.
- Yaron Lipman, Daniel Cohen-Or, David Levin, and Hillel Tal-Ezer. 2007. Parameterization-free projection for geometry reconstruction. In *ACM Transactions on Graphics (TOG)*, Vol. 26. ACM, 22.
- Hsueh-Ti Derek Liu, Vladimir G. Kim, Siddhartha Chaudhuri, Noam Aigerman, and Alec Jacobson. 2020. Neural Subdivision. *ACM Trans. Graph.* 39, 4 (2020).
- Krishna Murthy, Edward Smith, Jean-Francois Lafleche, Clement Fuji Tsang, Artem Rozantsev, Wenzheng Chen, Tommy Xiang, Rev Lebaredian, and Sanja Fidler. 2019. Kaolin: A PyTorch Library for Accelerating 3D Deep Learning Research. *arXiv:1911.05063* (2019).
- Adam Paszke, Sam Gross, Soumith Chintala, Gregory Chanan, Edward Yang, Zachary DeVito, Zeming Lin, Alban Desmaison, Luca Antiga, and Adam Lerer. 2017. Automatic differentiation in pytorch. (2017).

- Charles R Qi, Hao Su, Kaichun Mo, and Leonidas J Guibas. 2017a. Pointnet: Deep learning on point sets for 3d classification and segmentation. In *Proceedings of the IEEE conference on computer vision and pattern recognition*. 652–660.
- Charles Ruizhongtai Qi, Li Yi, Hao Su, and Leonidas J Guibas. 2017b. Pointnet++: Deep hierarchical feature learning on point sets in a metric space. In *Advances in neural information processing systems*. 5099–5108.
- Nikhila Ravi, Jeremy Reizenstein, David Novotny, Taylor Gordon, Wan-Yen Lo, Justin Johnson, and Georgia Gkioxari. 2020. PyTorch3D. <https://github.com/facebookresearch/pytorch3d>.
- Tamar Rott Shaham, Tali Dekel, and Tomer Michaeli. 2019. SinGAN: Learning a Generative Model from a Single Natural Image. *arXiv preprint arXiv:1905.01164* (2019).
- Nicholas Sharp et al. 2019. Polyscope. [www.polyscope.run](http://www.polyscope.run).
- Assaf Shocher, Nadav Cohen, and Michal Irani. 2018. "zero-shot" super-resolution using deep internal learning. In *Proceedings of the IEEE Conference on Computer Vision and Pattern Recognition*. 3118–3126.
- Xianfang Sun, Paul L Rosin, Ralph Martin, and Frank Langbein. 2007. Fast and effective feature-preserving mesh denoising. *IEEE transactions on visualization and computer graphics* 13, 5 (2007), 925–938.
- Dmitry Ulyanov, Andrea Vedaldi, and Victor Lempitsky. 2018. Deep image prior. In *Proceedings of the IEEE Conference on Computer Vision and Pattern Recognition*. 9446–9454.
- Yue Wang, Yongbin Sun, Ziwei Liu, Sanjay E Sarma, Michael M Bronstein, and Justin M Solomon. 2019. Dynamic graph cnn for learning on point clouds. *ACM Transactions on Graphics (TOG)* 38, 5 (2019), 1–12.
- Erik Wijmans. 2018. Pointnet2 Pytorch. (2018). [http://github.com/erikwijmans/Pointnet2\\_PyTorch](http://github.com/erikwijmans/Pointnet2_PyTorch)
- Francis Williams, Teseo Schneider, Claudio Silva, Denis Zorin, Joan Bruna, and Daniele Panozzo. 2019. Deep geometric prior for surface reconstruction. In *Proceedings of the IEEE Conference on Computer Vision and Pattern Recognition*. 10130–10139.
- Shiyao Xiong, Juyong Zhang, Jianmin Zheng, Jianfei Cai, and Ligang Liu. 2014. Robust Surface Reconstruction via Dictionary Learning. *ACM Trans. Graph.* 33, 6, Article Article 201 (Nov. 2014), 12 pages. <https://doi.org/10.1145/2661229.2661263>
- Wang Yifan, Shihao Wu, Hui Huang, Daniel Cohen-Or, and Olga Sorkine-Hornung. 2019. Patch-based progressive 3d point set upsampling. In *Proceedings of the IEEE Conference on Computer Vision and Pattern Recognition*. 5958–5967.
- Lequan Yu, Xianzhi Li, Chi-Wing Fu, Daniel Cohen-Or, and Pheng-Ann Heng. 2018a. Ec-net: an edge-aware point set consolidation network. In *Proceedings of the European Conference on Computer Vision (ECCV)*. 386–402.
- Lequan Yu, Xianzhi Li, Chi-Wing Fu, Daniel Cohen-Or, and Pheng-Ann Heng. 2018b. Pu-net: Point cloud upsampling network. In *Proceedings of the IEEE Conference on Computer Vision and Pattern Recognition*. 2790–2799.
- Yang Zhou, Zhen Zhu, Xiang Bai, Dani Lischinski, Daniel Cohen-Or, and Hui Huang. 2018. Non-stationary texture synthesis by adversarial expansion. *arXiv preprint arXiv:1805.04487* (2018).